SANDIA REPORT

SAND2013-8618
Unlimited Release
Printed October 2013

Towards understanding of Nipah virus attachment protein assembly and the role of protein affinity and crowding for membrane curvature events

Jeanne C. Stachowiak, Carl C. Hayden, Oscar A. Negrete, Ryan Davis, and Darryl Y. Sasaki

Prepared by
Sandia National Laboratories
Albuquerque, New Mexico 87185 and Livermore, California 94550

Sandia National Laboratories is a multi-program laboratory managed and operated by Sandia Corporation, a wholly owned subsidiary of Lockheed Martin Corporation, for the U.S. Department of Energy's National Nuclear Security Administration under contract DE-AC04-94AL85000.

Approved for public release; further dissemination unlimited.

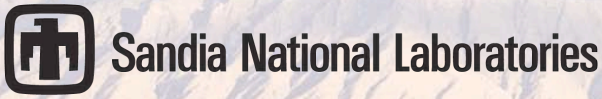

Issued by Sandia National Laboratories, operated for the United States Department of Energy by Sandia Corporation.

NOTICE: This report was prepared as an account of work sponsored by an agency of the United States Government. Neither the United States Government, nor any agency thereof, nor any of their employees, nor any of their contractors, subcontractors, or their employees, make any warranty, express or implied, or assume any legal liability or responsibility for the accuracy, completeness, or usefulness of any information, apparatus, product, or process disclosed, or represent that its use would not infringe privately owned rights. Reference herein to any specific commercial product, process, or service by trade name, trademark, manufacturer, or otherwise, does not necessarily constitute or imply its endorsement, recommendation, or favoring by the United States Government, any agency thereof, or any of their contractors or subcontractors. The views and opinions expressed herein do not necessarily state or reflect those of the United States Government, any agency thereof, or any of their contractors.

Printed in the United States of America. This report has been reproduced directly from the best available copy.

Available to DOE and DOE contractors from
U.S. Department of Energy
Office of Scientific and Technical Information
P.O. Box 62
Oak Ridge, TN 37831

Telephone: (865) 576-8401
Facsimile: (865) 576-5728
E-Mail: reports@adonis.osti.gov
Online ordering: http://www.osti.gov/bridge

Available to the public from
U.S. Department of Commerce
National Technical Information Service
5285 Port Royal Rd.
Springfield, VA 22161

Telephone: (800) 553-6847
Facsimile: (703) 605-6900
E-Mail: orders@ntis.fedworld.gov
Online order: http://www.ntis.gov/help/ordermethods.asp?loc=7-4-0#online

SAND2013-8618
Unlimited Release
Printed October 2013

Towards understanding of Nipah virus attachment protein assembly and the role of protein affinity and crowding for membrane curvature events

Jeanne C. Stachowiak[1,4], Carl C. Hayden[2], Oscar Negrete[1], Ryan Davis[3], and Darryl Y. Sasaki[1]

[1]Biotechnology & Bioengineering Department
[2]Combustion Chemistry Department
[3]Biomass Science & Conversion Technology Department
[4]University of Texas, Austin, Department of Biomedical Engineering

Sandia National Laboratories
P.O. Box 969
Livermore, CA 94551-MS 9292

Abstract

Pathogenic viruses are a primary threat to our national security and to the health and economy of our world. Effective defense strategies to combat viral infection and spread require the development of understanding of the mechanisms that these pathogens use to invade the host cell. We present in this report results of our research into viral particle recognition and fusion to cell membranes and the role that protein affinity and confinement in lipid domains plays in membrane curvature in cellular fusion and fission events. Herein, we describe 1) the assembly of the G attachment protein of Nipah virus using point mutation studies to define its role in viral particle fusion to the cell membrane, 2) how lateral pressure of membrane bound proteins induce curvature in model membrane systems, and 3) the role of membrane curvature in the selective partitioning of molecular receptors and specific affinity of associated proteins.

ACKNOWLEDGMENTS

This work was funded under LDRD Project Number 151349 and Title “Host-Virus Interaction Using an Artificial Host Cell System”. Additional funding was provided by NIH (grant AI069317), the NIH NIGMS and Nanomedicine Development Centers, the Miller Institute for Basic Research in Science, and the US Department of Energy, Office of Basic Energy Sciences, Division of Materials Science and Engineering and Division of Chemical Sciences, Geosciences, and Biosciences.

CONTENTS

FIGURES

NOMENCLATURE

DOGS-NTA-Ni	1,2-Dioleoyl-*sn*-glycero-3[(N-(5-amino-1-carboxypentyl)iminodiacetic acid)succinyl] nickel salt
DOIDA	1,2-Dioleyl-*rac*-glycero-3-triethyleneglycyl iminodiacetic acid
DOPC	1,2-Dioleoyl-*sn*-glycero-3-phosphocholine
DPPC	1,2-Dipalmitoyl-*sn*-glycero-3-phosphocholine
DPhPC	1,2-Diphytanoyl-*sn*-glycero-3-phosphocholine
DSIDA	1,2-Distearyl-*rac*-glycero-3-triethyleneglycyl iminodiacetic acid
FLIM	Fluorescence lifetime imaging microscopy
FRET	Förster resonance energy transfer
GFP	Green fluorescence protein
GUV	Giant unilamellar vesicle
HNV-G	Henipah virus G protein
IDA	Iminodiacetic acid
L_d	Liquid disordered
L_o	Liquid ordered
MeV	Measles virus
NiV	Nipah virus
NiV-G	Nipah virus G attachment protein
NDV	Newcastle disease virus
NTA	Nitrilotriacetic acid
PDMS	Polydimethylsiloxane
PMMA	Polymethylmethacrylate
POPC	1-Palmitoyl-2-oleoyl-*sn*-glycero-3-phosphocholine
SDS-PAGE	Sodium dodecylsulfate polyacrylamide gel electrophoresis
SEM	Scanning electron microscopy
wtENTH	wild type ENTH
DOE	Department of Energy
SNL	Sandia National Laboratories
NIH	National Institutes of Health

1. INTRODUCTION

The overarching idea behind this research was to reconstruct cellular mechanisms in a simplified synthetic environment to improve fundamental understanding of pathogen invasion. In order to infect host cells, pathogens must employ specific biochemical strategies to deliver their genetic material across host lipid membranes, formidable biochemical barriers that are impermeable to macromolecules. The initial events of infection by enveloped viruses include (i) attachment to receptors on the host cell surface, (ii) protein-mediated fusion of the host and virus lipid membranes, and (iii) release of the virus genetic material into the cell resulting in the onset of viral replication (**Fig. 1**). As the gateway to infection, these early events are attractive targets for therapeutic intervention and assay development.

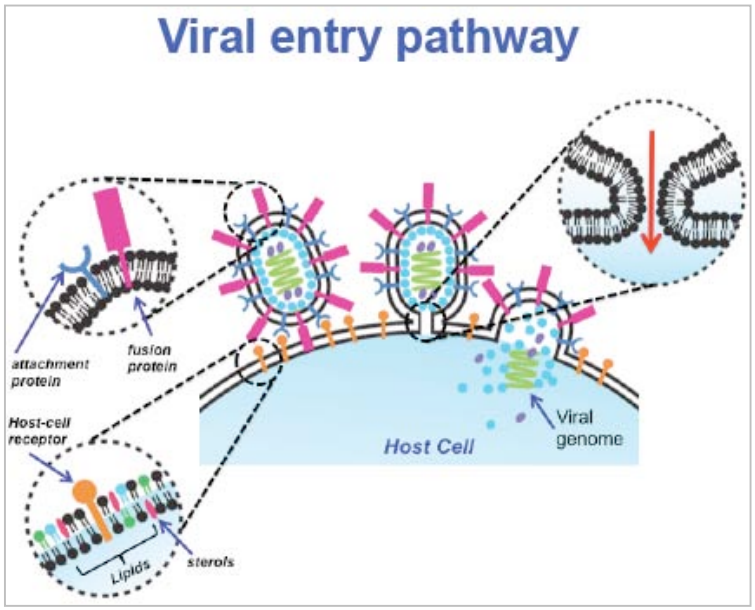

Figure 1. Viral entry into cells involves recognition and fusion events driven by protein assembly and remarkable changes in membrane curvature.

Cell studies frequently identify candidate host cell receptors, but questions of redundancy and sufficiency complicate design of countermeasures. In the study of living cells, key factors including lipid composition, membrane protein content, and membrane physical state (tension, curvature, fluidity) cannot be isolated. To examine the fundamental biochemical and biophysical requirements necessary for viral entry into host cells, we have examined the role of protein-membrane interactions on viral affinity and fusion to model and live cell membranes, explored the relationship between protein crowding on the membrane surface to induce curvature, and

examined how membrane curvature itself can direct the affinity of proteins and subsequent function to those assemblies. In this report, we will describe our findings of 1) the assembly of the G attachment protein stalk domain of the highly pathogenic Nipah virus (NiV) and their role in viral particle affinity and fusion to cell membranes,[1] 2) the role of lateral pressure of membrane bound proteins in generating curvature in model membrane systems and consider their importance in the fusion and fission of vesicles from cell membranes,[2] and 3) the influence of membrane curvature on receptor and protein partitioning in model membrane systems containing phases of different bending rigidities.[3]

2. RESULTS AND DISCUSSIONS

2.1. Cysteines in the stalk of the Nipah virus G glycoprotein are located in a distinct subdomain critical for fusion activation[1]

2.1.1. Background

Nipah virus (NiV) is an emergent, highly pathogenic, zoonotic agent classified as a risk group 4 pathogen.[4] NiV and Hendra virus (HeV) share the genus, *Henipavirus*, within the subfamily *Paramyxovirinae*. NiV was originally identified in 1999 as the infectious agent responsible for causing severe encephalitis and respiratory disease in humans and livestock in Malaysia.[5,6,7] This emergent zoonotic disease has spread to Singapore, India, and Bangladesh with recurrent outbreaks continuing in Bangladesh almost yearly for the last decade. Cited causes of NiV infections in Bangladesh include drinking contaminated palm date juice and close contacts of individuals with pteropid fruit bats, considered as the natural reservoir host.[8,9,10] What was first seen as a disease with little to no human-to-human transmission is now known to have a human-to-human transmission of approximately 50% in recent outbreaks with mortality rates up to 70%.[11] With no effective treatments available, it is essential to better understand the fundamental mechanisms of infection to aid the design of efficacious therapeutics.

To initiate paramyxovirus entry into target cells, the viral lipid membrane must merge with the cell membrane.[12,13,14] To overcome the energy barrier required for viral and cell membrane mixing, paramyxoviruses have evolved the use of two surface glycoproteins to drive fusion. One glycoprotein, the attachment protein, functions in recognition and binding to cellular receptors. Receptor binding results in allosteric triggering of the second protein, termed the fusion (F) protein, which is responsible for fusion of viral envelopes with cell membranes. The F

protein shares structural similarities classically described for the class I fusion proteins of Influenza and HIV. The trimeric mature F protein requires cleavage of the precursor F_0 protein into disulfide-linked F_1/F_2 subunits, which is held in a metastable conformation prior to fusion. Triggering the F protein during fusion results in drastic structural transitions, first involving the insertion of a hydrophobic fusion peptide into the host membrane and ends in folding of the N- and C-terminal α-helical heptad repeat (HR) domains within each trimer in a process termed six-helix bundle formation. The post-fusion F conformation is a highly stable and irreversible state.

Paramyxovirus attachment proteins are designated as HN, H or G depending on their hemagglutinin (H) and/or neuraminidase activity (N). The HN attachment protein of Newcastle disease virus (NDV) and most paramyxoviruses bind and cleave sialic acid moieties, while H and G proteins bind to protein receptors. Even though the H attachment protein of *morbilliviruses* such as Measles virus (MeV) binds to protein-based receptors, they retain hemagglutinin activity, albeit through binding of its protein receptor rather than through sialic acid. Unlike other paramyxoviruses, the henipavirus G attachment proteins (HNV-G) are devoid of both hemagglutinin and neuraminidase function but bind to cellular receptors ephrinB2 and ephrinB3.[15,16,17] Paramyxovirus attachment proteins are all type II integral membrane proteins that form non-covalently associated tetramers consisting of dimer-of-dimers that are typically covalently linked within, but not between each dimer. The C-terminal globular head or receptor binding domain connects to the N-terminal cytoplasmic tail and transmembrane region through a highly flexible stalk domain. Crystal structures of the NiV-G and HeV-G globular domain reveal the characteristic six-bladed beta-propeller seen in other paramyxovirus HN and H structures.[18,19] Regions of the HN stalk domains for NDV and parainfluenza virus 5 (PIV5) recently crystallized show a parallel tetrameric α-helical coiled-coil configuration simply termed

a four-helix bundle (4HB).[20,21] Although structural information for the H or G attachment protein stalk domains does not exist, secondary structure predictions and alignments support the existence of a similar α-helical structure.[22,23]

HNV-G proteins contain a distinct cluster of three cysteine residues (C146, C158, C162) located in a distal portion of the stalk domain (**Fig. 2**). Cysteines in the stalk domain of HN/H proteins have a pivotal role in disulfide-linked dimerization. However, the removal of these intermolecular disulfide bonds does not eliminate the fusion triggering capabilities of either HN or H.[24,25] Stalk extension in the MeV H protein also indicates that the location of these disulfide bonds is not important in triggering, as residues inserted into a central stalk region heighten the position of the intermolecular bonds yet remain fusogenic.[26] In this study, we used mutagenesis to understand the role of cysteine residues in the Nipah virus G stalk. Our present analysis indicates that these cysteines not only play a role in stabilizing the oligomeric state of G through disulfide-linked dimerization, but also helps maintain G in a pre-receptor bound conformation. Additionally, the cysteine cluster in a distal section of the G stalk was found to lie near a proline-rich microdomain unique to the henipaviruses amongst *Paramyxovirinae* genera. We propose that the most important function of the cysteine cluster is ensuring the proper folding of the proline-rich microdomain critical to the conformational stability associated with F-triggering.

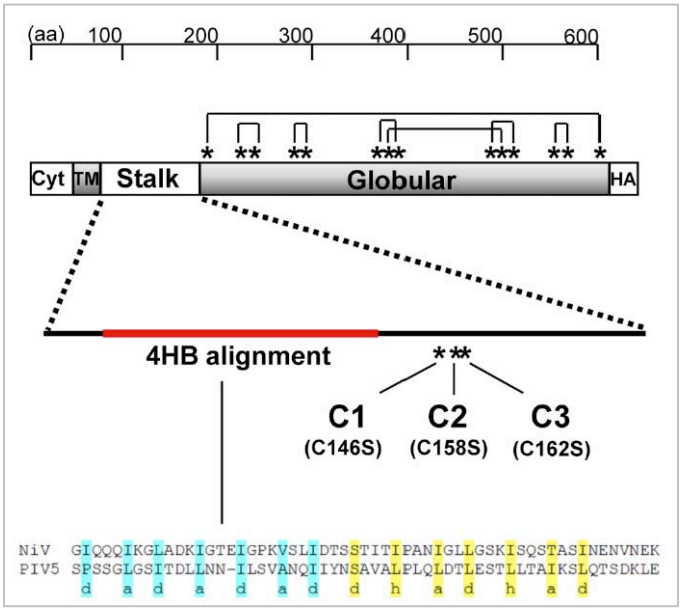

Figure 2. Schematic diagram of the locations of cysteine residues and intramolecular disulfide bonds in the NiV-G protein sequence.

2.1.2. Discussion

We used a panoply of assays to examine the role of stalk domain cysteine residues in maintaining the structure and function of NiV-G. Cysteine residues of secretory pathway proteins in general, can participate in disulfide bond formation during protein folding that serves to stabilize folding intermediates, as well as the mature protein architecture.[27] The NiV-G protein, with a total of 17 cysteine residues, forms 7 intramolecular disulfide bonds in the completely folded six-bladed beta-propeller structure. The three cysteine residues remaining are located in the stalk and have not been previously characterized for their functional role in oligomerization or fusion promotion. Similar to other paramyxovirus systems, we found that cysteines in the stalk of NiV-G assist in maintaining oligomeric stability by participating in intersubunit disulfide bond formation. However, in contrast to HN or H attachment proteins where cysteine mutations in stalk domain at most attenuate fusion, we found that mutations of cysteine residues in the NiV-G stalk domain were completely fusion deficient.

It remains unclear whether C158 and C162 participate in the formation of a single or multiple intersubunit disulfide bonds. We speculate that due to the proximity of these two cysteine residues, C158 and C162 first form an intramolecular disulfide bond to protect these reactive thiols during protein folding. In the later stages of G folding, this intramolecular bond would isomerize to form a single or, most likely, double intermolecular disulfide bonds.[27] In this scenario, the C2 and C3 mutants, which lack either C158 or C162 thiols, respectively, cannot form the early intramolecular bond between C158 and C162: thus, they are prevented from isomerization and intersubunit disulfide bond formation, an idea consistent with the nonreducing SDS-PAGE results (**Fig. 3**). Additionally, the absence of tetramers in mutant C1 under nonreducing conditions suggests that another intersubunit disulfide bond, which functions to stabilize the tetramer in wild-type G, may exist across NiV-G dimer pairs. Lastly, the fact that mutants C2 and C3 were completely monomeric under nonreducing conditions suggests that intersubunit bond formation at position C146 is dependent on the prior formation of the C158/C162 intersubunit bond(s). A model for HNV-G disulfide linkage in the stalk domain is shown in **Figure 4**.

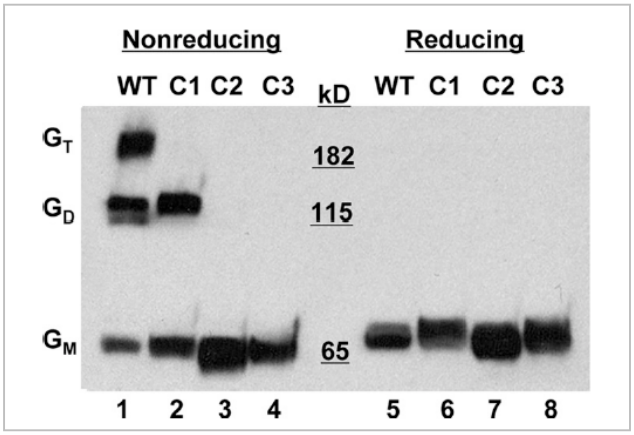

Figure 3. Western blot analysis of cysteine mutants under reducing and non-reducing conditions.

Other than henipaviruses whose stalk are approximately 40 amino acids greater in length than most HN proteins, morbillivirus attachment proteins also contain extended stalk domains compared to typical HN stalk (MeV H stalk has 120aa). Upon assessment of stalk domain sequences across the *morbillivirus* genus, it was apparent that the H stalk could be divided into

similar subdomains as indicated by functional studies of HNV-G proteins . As for *henipavirus* G, subdomains I and IV in *morbillivirus* H are less conserved that subdomains II and III. The H stalk subdomain II also contains the aligned 4HB region, while the subdomain III contains cysteines important for intersubunit disulfide linked dimerization.[28] Interestingly, despite similar stalk lengths, alignment of subdomains III and IV of henipaiviruses to morbilliviruses highlighted a unique proline-rich microdomain present only in the henipavirus stalk. Although the exact function of the proline-rich microdomain in the HNV-G stalk remains to be understood, future studies using chimeras of stalk subdomains between MeV-H and NiV-G is likely to be revealing. Since MeV-H and HNV-G differ in their site of receptor engagement, at the side or at the top of the six bladed beta-propeller for MeV-H and HNV-G, respectively, we speculate that the proline-rich microdomain plays a unique role in transmitting the receptor induced allosteric signals to effectuate fusion triggering. Future biochemical and chimeric studies may answer these and other questions regarding the similarities and differences in the fusion mechanisms of across paramyxoviruses.

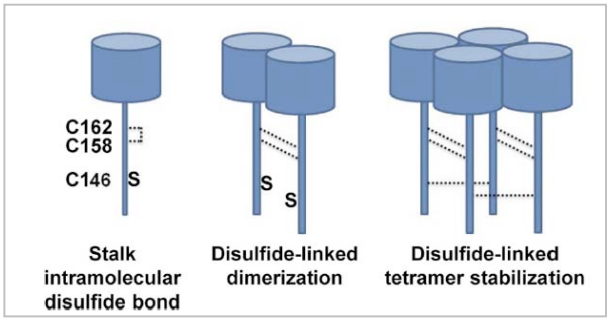

Figure 4. Model of henipavirus G stalk domain disulfide bond formation. The G protein globular domain is represented as a cylinder and the stalk domain as a stick.

In all, we showed that cysteines in the stalk domain of NiV-G are not only important for maintaining the oligomeric stability of G, but also for proper folding of a unique subdomain located in the membrane distal region of the stalk that is necessary for F-triggering. This subdomain is critical for maintaining the G in its pre-receptor bound conformation, and although it is essential for F triggering, it is not necessary for stable F interactions. These studies supplement our knowledge on the function of the stalk domain of paramyxovirus attachment

proteins in F triggering, and identifies a critical microdomain that can be targeted for therapeutic or vaccine development.

2.2. Membrane bending by protein-protein crowding[2]

2.2.1. Background

Highly curved cellular membranes are thought to form by two distinct mechanisms. First, intrinsically curved proteins[29] and oligomers[30] can drive bending, though their ability to do so independently has been debated.[31,32] Second, insertion of amphipathic helices is thought to bend membranes through a wedge-like mechanism.[33,34] Clathrin-mediated endocytosis, the major endocytic pathway in eukaryotic cells, requires a network of interacting proteins, several of which have been implicated in membrane bending.[35] Central among these, Epsin1 is thought to be capable of driving curvature generation in clathrin-coated pits.[33] Our work tests the currently accepted hypothesis that Epsin1 bends membranes by helix insertion and finds instead that protein-protein crowding drives membrane bending.

The N-terminal homology region of Epsin1 (ENTH domain) attaches to the membrane by binding $PI(4,5)P_2$ lipids and inserting an amphipathic helix (helix0) into its cytoplasmic leaflet.[33] Epsin 1, has been shown to have a cargo sorting role,[36] to act as a curvature sensor,[37] and to bind multiple endocytic proteins via its flexible C-terminus,[38] all of which likely assist in its localization to endocytic sites. Since ENTH has no inherent curvature with which to influence membrane shape, it has been thought that insertion of helix0 increases the membrane's outer leaflet area, causing convex curvature. This hypothesis, originally proposed for Epsin1 ENTH domain and subsequently termed hydrophobic insertion, has been used to explain the role of amphipathic insertion motifs in proteins relevant to a wide range of topics in cell biology,

including viral entry,[39] apoptosis,[40] autophagy,[41] vesicular traffic,[34] and motility.[42] Supporting this hydrophobic insertion hypothesis, the N-terminal homology domain of AP180 (ANTH domain), which is structurally similar to the ENTH domain but missing the helix, has not been found to generate curvature.[43]

While helix insertion is expected to increase the area of one leaflet of the bilayer, it is unclear whether that increase is sufficient to generate high curvatures, given that helix density is limited by the size and coverage of the protein containing the helix.[44] Recently, continuum models[45] and molecular dynamics simulations[46] have predicted that helix insertions alone must occupy 10-25% of the membrane surface area in order to generate the curvatures found in endocytic structures. For Epsin ENTH, however, the helix insertion (~8 Å wide × 20 Å long ≈ 1.6 nm^2) takes up at most 10% of the ENTH domain's membrane footprint (~40 Å × 40 Å ≈ 16 nm^2). Therefore, even in the physiologically unlikely case that these proteins cover 100% of the membrane surface, the helix can occupy at most 10% of the membrane surface area, still at the lower end of the helix density that computational models estimate is required to drive high curvatures. Furthermore, the maximum helix density is even less if the significantly larger full-length Epsin1 protein is considered.

2.2.2. Discussion

Since Epsin ENTH has been shown to generate high curvatures in vitro, we set out to measure the surface coverage required. We exposed electroformed giant unilamellar vesicles (GUVs) to wild type ENTH (wtENTH) and quantified the percentage of vesicles forming tubules. Then, we correlated these results with fluorescence lifetime based Förster resonance energy transfer (FLIM-FRET) measurements of the density of membrane-bound wtENTH

participating in membrane bending. GUVs employed a lipid composition that phase separated at room temperature into a liquid-ordered majority phase containing a small liquid-disordered domain in which the $PI(4,5)P_2$ was concentrated.[47] The density of protein binding to membrane surfaces was varied by changing the $PI(4,5)P_2$ concentration in the fluid membrane regions of the GUV.

When exposed to the GUVs, wtENTH rapidly bound to the initially flat $PI(4,5)P_2$-enriched domains (**Fig. 5**), and, in the case of high $PI(4,5)P_2$ concentrations, produced protein-coated lipid tubules that frequently consumed much of the domain area (**Fig. 5b**). Tubules had diffraction-limited diameters and appeared highly flexible, fluctuating rapidly in conformation and often displaying a pearled morphology. Pearled tubules have been previously observed for membranes with high spontaneous curvature,[48] suggesting that protein attachment increases spontaneous curvature. Similar tubules were observed for alternative systems of fluid lipids that also contained $PI(4,5)P_2$, both with and without phase separated domains, showing that this behavior is not limited to the chosen lipid mixture. Tubules were not present in the

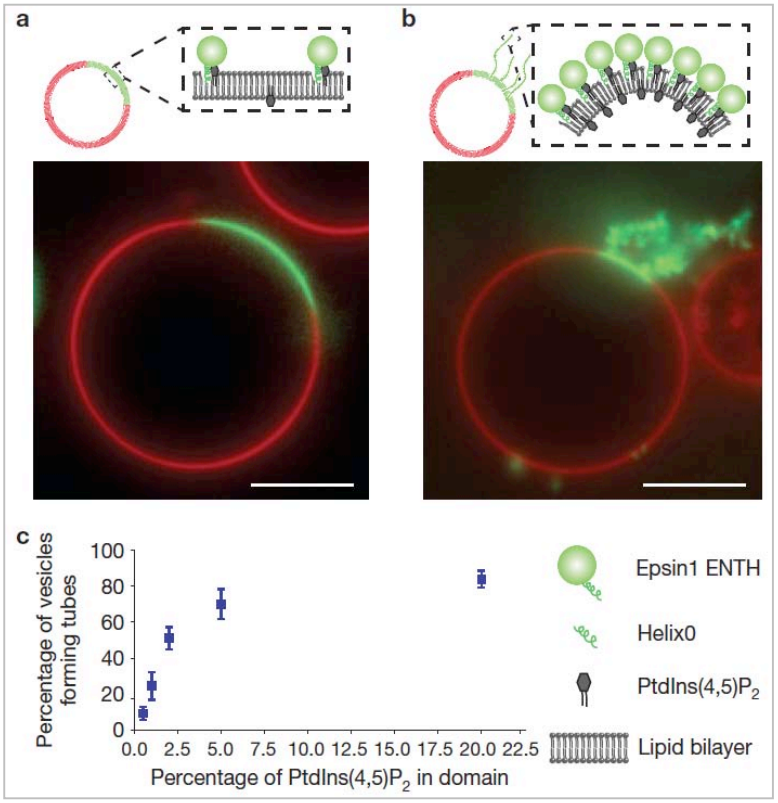

Figure 5. $PtdIns(4,5)P_2$ concentration in membranes controls the frequency of lipid tubule formation by epsin1. Binding of Atto488 labeled wt-ENTH (green) at a) low (~2 mole %) and b) high (~20 mole %)concentration of $PtdIns(4,5)P_2$. c) Graph of percentage of tubules formed as a function of $PtdIns(4,5)P_2$ in membrane domains.

absence of proteins, regardless of membrane composition. In our experiments, the percentage of vesicles having observable tubules was found to depend strongly on the molar fraction of $PI(4,5)P_2$ included in the membrane domain, increasing from 9 +/- 4% s.d. (for 0.5 mol% $PI(4,5)P_2$) to 84 +/- 5% s.d. (with 20 mol% $PI(4,5)P_2$ (**Fig. 5c**). As expected, no protein attachment to membranes was observed in the absence of $PI(4,5)P_2$.

We determined the density of membrane-bound proteins responsible for the observed tubulation by measuring FRET between dye-labeled proteins on the membrane surface. Using this assay, we quantified the percentage of the membrane covered by wtENTH as a function of increasing $PI(4,5)P_2$ concentration (**Fig. 6**). Separate donor and acceptor-labeled protein populations mixed in a 1:5 ratio (1 μM total wtENTH) were exposed to the same GUVs used for determining the frequency of tubulation (0.5 - 20 mol% PI(4,5)P2 in domains). As the overall protein surface density was increased, by increasing the concentration of $PI(4,5)P_2$, the density of acceptors around each donor increased, leading to quenching of the donor fluorescence via Förster resonance energy transfer to the acceptors (**Fig. 6a,b**). The donor and acceptor lifetimes were recorded using confocal

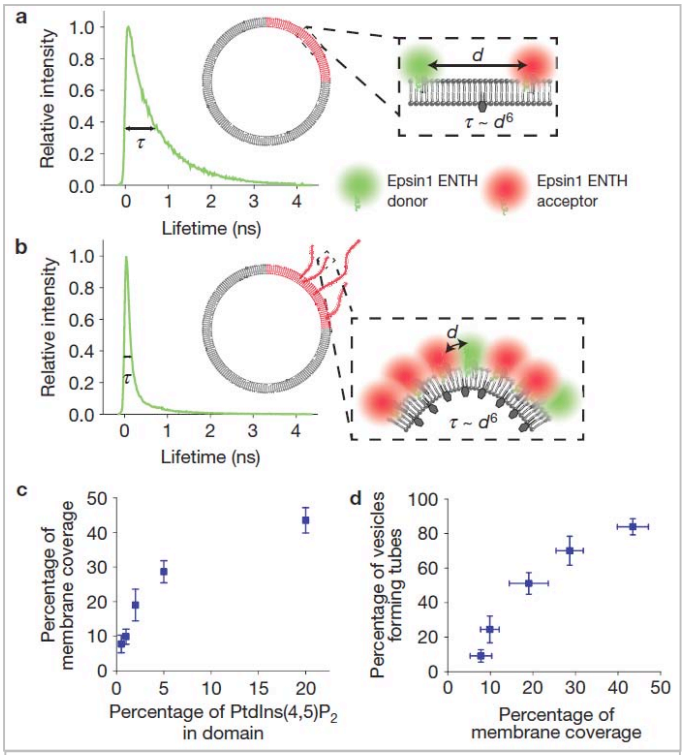

Figure 6. FLIM-FRET meaurements of epsin1 density reveal that PtdIns(4,5)P_2 concentration controls protein coverage of membrane surfaces. τ – lifetime of FRET donor fluorophore, d – separation between donor and acceptor. wt-ENTH labeled with donor (Atto532/560) and acceptor (Atto594/627) at a) low and b) high protein coverage affects τ. Graphs show c) membrane coverage by proteins as a function of PtdIns(4,5)P_2 concentration in domains and d) frequency of tubule formation as a function membrane coverage by wtENTH.

fluorescence lifetime imaging microscopy, providing images of local donor lifetimes. If protein oligomerization occurred, we would expect to see short lifetimes even at moderate densities. However, our experiments are accurately modeled by a random distribution of proteins at all densities, indicating no evidence of oligomerization, in contrast to a recent report.[49]

We found that average coverage area increased proportionally from 8 +/- 3% s.d. coverage (1 protein every 200 nm^2) at 0.5 mol% $PI(4,5)P_2$ to 29 +/- 3% s.d. coverage (1 protein every 50 nm^2) at 5 mol% $PI(4,5)P_2$ and that coverage area increased more slowly up to 45 +/- 4% s.d. coverage (1 protein every 32 nm^2) at 20 mol% $PI(4,5)P_2$, likely due to saturation of the membrane surface with proteins.[50] Combining these data with the measurements in **Figure 5** reveals a strong correlation between the frequency of tubule formation and the percentage of the membrane domain area covered by proteins. When wtENTH molecules cover approximately 20% of the domain area, half of the vesicles form tubules (**Fig. 6d**). At this threshold, however, inserted helices (estimated as 10% of the ENTH footprint) covered only 2% of the domain surface area (less than one helix per 100 lipids, about 70 nm^2), far below the 10-25% surface area coverage predicted to be necessary for generating high curvature by hydrophobic insertion.[45,46]

These results call into question the ability of helix insertion to drive the observed membrane bending by ENTH. We therefore sought to measure the capacity of ENTH to bend membranes in the absence of insertions. We replaced helix0 in wtENTH with an engineered hexa-his tag (hisENTH) and replaced $PI(4,5)P_2$ with DOGS-NTA-Ni (4 – 20 mol%) in the GUVs. This attachment chemistry provides a high affinity protein-lipid interaction, $K_d \sim$ nM, via binding of the histidine residues to the DOGS-NTA-Ni lipid heads,[51] rather than via helix insertion. Upon exposure to the GUVs, hisENTH bound to the DOGS-NTA-Ni enriched membrane domains, producing tubules at high DOGS-NTA-Ni concentrations that appeared

morphologically indistinguishable from those formed by wtENTH binding to PI(4,5)P_2-enriched domains (**Fig. 7**). As with wtENTH, the frequency of tubule formation and membrane surface coverage by hisENTH was measured with the fluorescence lifetime based FRET technique and found to increase strongly with increasing DOGS-NTA-Ni concentration.

Cellular membranes are known to be densely populated with transmembrane and membrane-binding proteins,[52] but the physiological implications of this crowded environment are just beginning to be explored. Our observation of density-dependent tubulation by ENTH domains, ANTH domains, and membrane-bound GFP suggest a general mechanism by which steric congestion on cellular membranes could assist in curvature generation. Specifically, since protein crowding at the membrane surface drives bending away from the adhered proteins, the balance between lateral pressures on each surface of the membrane could determine its shape, such that regions curved in either direction could arise from local asymmetries in protein density.

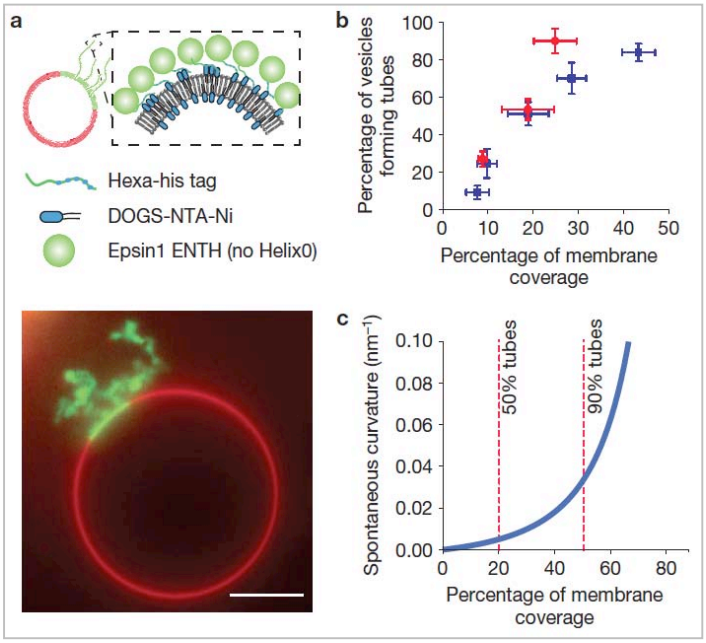

Figure 7. Protein coverage controls tubule formation regardless of membrane attachment chemistry. a) Schematic and fluorescence image of his-tagged ENTH labeled with Atto488 binds to membrane domains containing DPhPC and DOGS-NTA-Ni in a GUV of DPPC. B) Frequency of tubule formation as a function of membrane coverage by hisENTH [1 μM] (red circles) compared against wtENTH bound to PtdIns(4,5)P_2 (blue squares). Graph c) shows the predicted (blue line) spontaneous curvature (1/radius) as a function of coverage for protein-protein crowding model along with red dashed line representing the experimental values for 50% and 90% of vesicles that form tubules.

2.3. Patterning of Membrane-Bound Proteins through Curvature-Induced Partitioning of Phase-Specific Receptor Lipids[3]

2.3.1. Background

Lipid mixtures self-assemble to form planar bilayers containing coexisting lipid phases in many compositional regimes.[53,54] Coexisting lipid phases each have distinct compositions that can selectively partition optically active dyes, ligands, and membrane proteins.[55,56,57] Therefore, precise arrangements of these phases in continuous lipid bilayers could be used to create displays of proteins, DNA strands, optically, chemically, or electrically active molecules, or nanoparticles. Such displays could offer an extremely high-density array of active molecules or particles with functionality similar to a liquid crystal display. In contrast, most lipid bilayer patterning techniques form compositionally well defined, but disconnected, patches of lipid bilayers.[58,59]

Curvature-based sorting of functionalized lipids that comprise or partition into specific lipid phases could serve as a way of templating active molecules. Curvature-based sorting of coexisting lipid bilayer phases of differing compositions has been studied using substrate imposed curvature. Surface features presenting varying curvature and ridges with varying angles, formed by standard photolithography, have been used to impose curvature on coexisting liquid ordered (L_o) and liquid disordered phases (L_d). Partitioning of the stiffer L_o phase domains to the flatter surfaces took place above a certain threshold in the curvature or the ridge angle.[60,61] Similarly, wrinkled and templated PDMS have been used to demonstrate curvature sorting of lipid phases.[62,63] More recently, curvature thresholds were demonstrated for curvature sensing proteins using membrane-coated channel patterns created by photolithography.[64] We showed that nanometer-scale lipid sorting patterns are possible using an underlying substrate containing a

square lattice pattern of hemispherical features, formed by standard e-beam lithography of a poly(methyl methacrylate) (PMMA) layer on silica.[65] The high-bending modulus (~6×10^{-19}J)[66] L_o phase formed the fundamental units (or "pixels") of the pattern by being confined to and centered on the flat region between the unit cell of 4 hemispheres and these "domain pixels" connected up to form linear and rectangular two-dimensional shapes surrounded by the lower bending modulus (~1×10^{-19}J)[67] L_d phase. We quantitatively showed that this initial domain pattern shape is driven by a lowered bending energy, where the L_o phase avoids the high curvature (~10 μm^{-1}) of the 200 nm projected diameter hemispheres, which is larger than the increase in line energy associated with interconnected domain pixels.

A variety of methods have been developed to attach functional molecules to lipid headgroups. These include covalent bonding[68] and linkers such as single-stranded DNA,[69] biotin,[70] and glycan-phosphatidyl inositol.[71] Lipid headgroups can also be functionalized with a metal chelate group such as iminodiacetic acid (IDA)[72] or nitrilotriacetic acid (NTA).[73] These chelate groups coordinate to divalent transition-metal ions such as Cu^{2+}, Ni^{2+}, and Zn^{2+} and sequester proteins rich with histidine moieties. The phase behavior of the IDA-lipid can be varied by the length and unsaturation of the lipid tails. For example, we have shown that in the presence of Cu^{2+}, Cu^{2+}-DSIDA containing two saturated stearoyl chains forms a condensed gel-like $L_{\beta'}$ phase at room temperature and Cu^{2+}-DOIDA containing two unsaturated oleoyl chains forms a fluid-like L_d phase at room temperature.[74] These IDA-functionalized lipids (structures shown in **Figure 8** have been used to localize the binding of a variety of histidine-tagged proteins to domains of a specific lipid phase predominantly in giant unilamellar vesicles (GUVs).[75,76] In addition, surface crowding of histidine (His)-tagged proteins have been shown to cause remarkable changes in membrane shape.[77]

Here we move this technology toward the applications mentioned in the first paragraph by targeting a histidine-tagged protein to membranes containing Cu^{2+}-IDA lipids that have been compositionally patterned by an underlying curvature patterned substrate. As in our previous work,[65] 40 μm × 40 μm regions of the substrate are imprinted with a 600 nm square lattice pattern of 200 nm PMMA hemispheres by e-beam lithography. On these patterned substrates, we form L_d - L_o or L_d - $L_{\beta'}$ phase-separated lipid multibilayers containing, respectively, Cu^{2+}-DOIDA which we expected to localize at the hemispherical lattice sites, or Cu^{2+}-DSIDA which we expected to localize between these lattice sites. Fluorescence microscopy is used to characterize the localization of Cu^{2+}-DOIDA or Cu^{2+}-DSIDA on these curvature patterns as well as their large-scale phase separation on a flat substrate. In addition, fluorescence microscopy is used to detect the location of histidine-tagged green fluorescent protein (His-GFP) bound to these compositionally distinct curvature patterned lipid multilayers. We show that it is possible to form a defect-free lattice pattern (array) of His-GFP with this method. We comment on variations in the His-GFP lattice pattern in relation to the ratio of curved area fraction to L_d area fraction and phase behavior of the lipids.

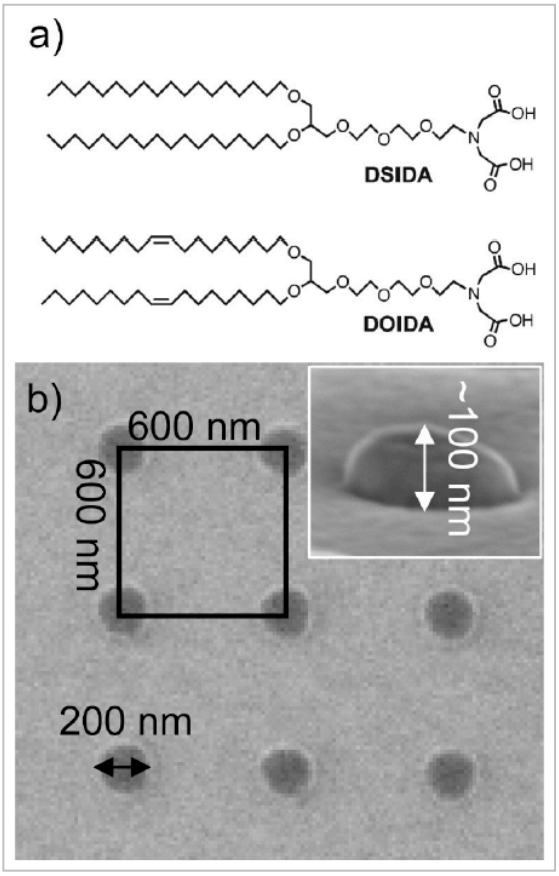

Figure 8. a) Structures of IDA-functionalized lipids, and b) SEM image of e-beam patterned substrate (inset shows hemisphere bumps at oblique angle.

2.3.2. Discussions

We began by demonstrating that we observe L_d - L_o phase separation in a hydrated lipid multibilayer formed from (20% Cu^{2+}-DOIDA/20% DOPC/60% DPPC)/20% cholesterol through spin coating onto a silicon wafer coated with 100 nm of PMMA and hydrating with a buffer containing 200 μM $CuCl_2$. By including 2% of a fluorescent probe (NBD-PC) that partitions with the L_d phase, we show (**Fig. 9a)** that this mixture formed large scale (1-10 μm) round dark domains typical of the L_o phase in coexistence with the brighter L_d phase. Typically we spin coat 2 to 3 bilayers and the distal 1 or 2 bilayers, respectively, display microscopically visible L_o phase, as previously reported by Simonsen et al.,[78] giving two shades of grey for overlapped and non-overlapped domains. As we have reported for a spin-coated (40% DOPC/60% DPPC)/20% cholesterol hydrated multibilayer, we observed coalescence of domains taking place over periods of seconds (**Fig. 9b**) which is a clear indication of liquid-liquid phase separation. The area fraction of the dark L_o phase was approximately 58%, in agreement with our previous measurement with (40% DOPC/60% DPPC)/20% cholesterol. These results suggest that Cu^{2+}-DOIDA partitions with DOPC in the L_d phase of this L_d - L_o phase separated multibilayer on an unpatterned substrate.

Next, we formed a hydrated multibilayer from (20% Cu^{2+}-DOIDA/20% DOPC/60% DPPC)/ 20% cholesterol/2% BODIPY on the curvature patterned substrates using spin coating followed by hydration with a buffer containing 200 μM $CuCl_2$ (**Figs. 9c,d**). Each curvature-patterned substrate used in this manuscript contains a 4 × 4 matrix of the same surface curvature pattern, each 40 μm × 40 μm in area. In each 40 μm × 40 μm area, there is a 600 nm × 600 nm square lattice pattern of PMMA hemispheres on flat silica as shown in the SEM image of **Figure 8b**. The curvature pattern was formed using electron beam lithography upon a 100 nm layer of

PMMA supported on a silicon wafer. **Figure 9c** shows the typical appearance of the L_d - L_o phase multibilayer supported by a 40 μm × 40 μm patterned area of the substrate. A large fraction of the multibilayer (center of **Fig. 9c**) clearly contained coexisting L_o phase (dark) and L_d phases (light). Moreover, within this region the position of the light L_d phase, which should contain Cu^{2+}-DOIDA, corresponds with the 600 nm center-to-center lattice spacing of the underlying hemispheres as shown by the dashed lines in **Figures 9d & 9e**. In comparison, the dark L_o phase is observed as forming an interconnected network between the lattice positions of L_d phase. This observation is in agreement with our previous patterning of (20% DOPC/60% DPPC)/20% cholesterol L_d - L_o multibilayers by the same underlying curvature lattice where we postulated the formation of an interconnected network of L_o "pixels" confined to the flat "grid" between the lattice sites of the hemispheres as shown by the schematic drawing overlaid on the SEM image in **Figure 9e** and with flat regions evident in **Figure 9f**. These results are strongly

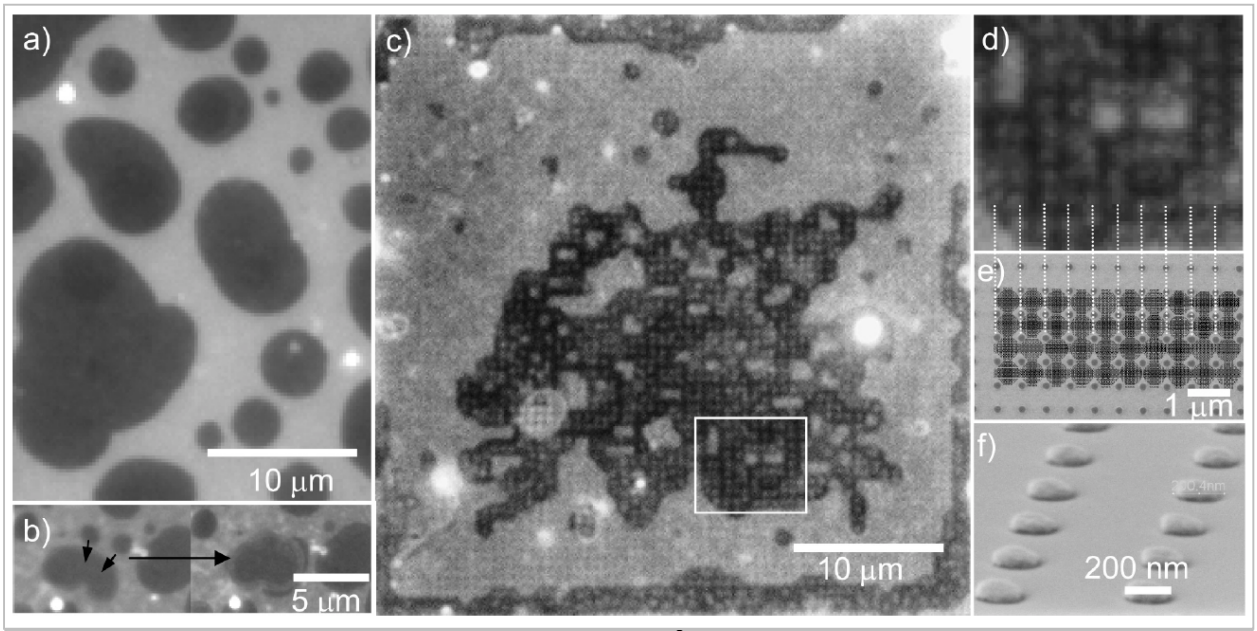

Figure 9. Phase separation of a multibilayer of (20% Cu^{2+}-DOIDA/20% DOPC/60% DPPC)/20% cholesterol/2% NBD-PC on a) flat PMMA (fluidity of the domains is demonstrated in (b)) and c) on a pattern of PMMA nanoscale bumps (200 nm diameter hemispheres arranged in a 600 nm square pattern). d) Magnified image of rectangular region in (c), and e) overlay images of SEM of bump pattern and drawing of interconnected pixel pattern of L_o phase. f) SEM image of underlying bump pattern.

indicative that the transfer of a curvature pattern to a compositional pattern is a viable way to position a functional group, i.e. the Cu^{2+}-IDA group associated with Cu^{2+}-DOIDA, on a substrate surface.

It has been established previously that His-GFP binds to the Cu^{2+}-IDA headgroup of Cu^{2+}-DOIDA.[76] Therefore, His-GFP should bind at the locations of the L_d-associated Cu^{2+}-DOIDA localized by the underlying hemispheres of the curvature pattern. For this experiment, the L_d phase was not labeled by any fluorescent probe so there could be no spectral overlap of the probe and the bound His-GFP. We added His-GFP to a multibilayer formed from spin-coated (20% Cu^{2+}-DOIDA/20% DOPC/60% DPPC)/20% cholesterol supported by the curvature patterned substrates (hydrated with buffer containing 200 μM $CuCl_2$). We observed the coexistence of dark and light regions in a significant area fraction of the 40 μm × 40 μm curvature patterned areas (**Fig. 10a**) as expected based upon the phase behavior of the lipid mixture and the localization of Cu^{2+}-DOIDA with the L_d phase. The position of the bright fluorescence associated with His-GFP corresponds with the 600 nm lattice spacing of the underlying hemispheres as shown by the dashed lines in Figure 10. In the dark regions, the continuous network geometry is evident as illustrated by comparing the image in Figure 10b to the illustration in Figure 10c. These

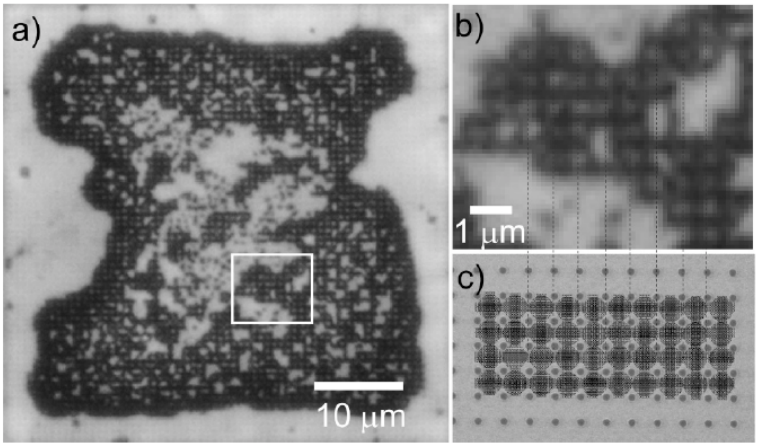

Figure 10. His-GFP binding to of phase separated domains in (20% Cu(II)-DOIDA/20% DOPC/60% DPPC)/20% cholesterol on nanoscale bump surface as in Figure 9. Fluorescence image in (a) and magnified view of rectangle shown in (b) reveals a pattern of pixels of bound GFP that are commensurate with (c) nano-bump pattern observed with SEM.

observations show that we can transfer a nanometer-scale pattern of curvature to a compositional pattern based upon membrane phase. Subsequently, the pattern can be transferred once again to a surface adsorbed protein (i.e., His-GFP) that binds specifically to a molecule (i.e., Cu^{2+}-DOIDA) associated with a particular phase (i.e., L_d).

By changing from the unsaturated tails of Cu^{2+}-DOIDA to the saturated tails of Cu^{2+}-DSIDA we move to a lipid in the gel phase at room temperature,[29] which provides an opportunity to localize the IDA functional group to the flat regions of the underlying curvature pattern. We formed a hydrated multibilayer from (15% Cu^{2+}-DSIDA/77% POPC/8% cholesterol)/2% NBD-PC supported on a curvature-patterned substrate. The multibilayer was formed by spin coating followed by hydration in a 200 μM $CuCl_2$ buffer. In analogy to the same composition of DSPC/POPC/cholesterol, this composition would be in the L_d - $L_{\beta'}$ coexistence region with similar partitioning of cholesterol to each phase. Cholesterol was included to provide some fluidity to the gel phase such that the multibilayer would conform when the underlying substrate contained the curvature patterned regions.

After visualizing the BODIPY pattern with fluorescence microscopy, we added His-GFP and imaged both the location of the BODIPY (red channel) that partitions with L_d phase and the His-GFP (green channel) with fluorescence microscopy. The BODIPY pattern was identical before and after binding His-GFP and therefore we only show the BODIPY pattern after binding His-GFP in **Figure 11**. In the red channel, dark $L_{\beta'}$ domains were observed on each section of the multibilayer supported by the underlying curvature lattice pattern as shown in Figure 4b. Within these dark domains were individual bright red spots with square lattice spacing of 600 nm matching the underlying lattice spacing of the hemispheres, indicating that domains of L_d phase (enriched in L_d phase POPC) were positioned above the hemispheres and the $L_{\beta'}$ phase (enriched

in Cu^{2+}-DSIDA) was positioned above the flat grid space between the lattice points as shown in the grayscale inset of Figure 11b. Visualizing these domains with both the red (BODIPY) and green (His-GFP) channels as shown in Figure 11c, we found that His-GFP occupies the flat grid space between the hemispherical lattice points, matching the general pattern of the dye-depleted $L_{\beta'}$ phase enriched in gel-phase Cu^{2+}-DSIDA (Figure 11b).

We demonstrated here that a nanometer-scale e-beam formed curvature pattern on a substrate can be transferred to a compositional pattern of functionalized lipid molecules, i.e. Cu^{2+}-IDA lipids, through curvature sorting of two lipid phases. Subsequently, the pattern can be transferred once again through binding of an active molecule, i.e. histidine-tagged green fluorescent protein, to the functionalized lipid. Cu^{2+}-DOIDA, which sorts with the L_d phase in L_d - L_o lipid multibilayers, was used to form an array of His-GFP pixels on hemispherical lattice sites of a 600 nm × 600 nm unit cell. Conversely, Cu^{2+}-DSIDA, which sorts

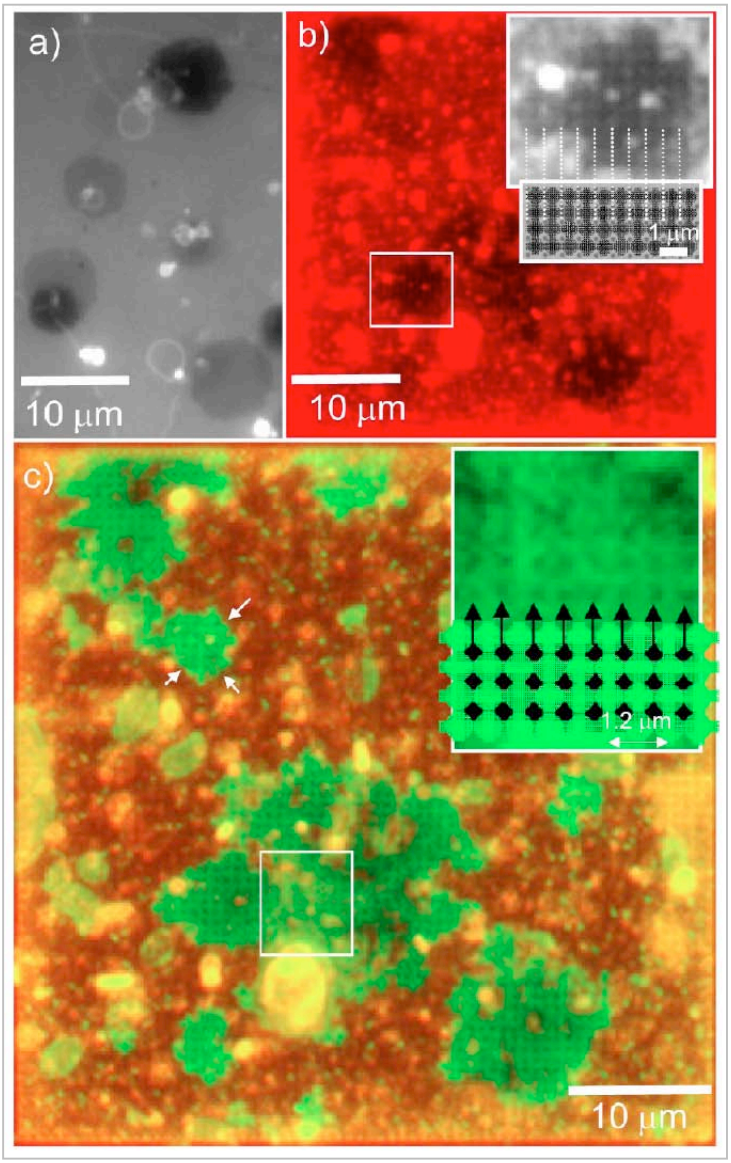

Figure 11. Phase separation of (15% Cu(II)-DSIDA/77% POPC/8% cholesterol)/2% NBD-PC as a multibilayer on a) flat PMMA, b) nanoscale bump surface, and c) after exposure to his-GFP.

with the $L_{\beta'}$ phase in L_d - $L_{\beta'}$ lipid multibilayers, was used to form a negative pattern of His-GFP in comparison, occupying the flat grid between the lattice sites of the 600 nm × 600 nm unit cell.

This page left blank intentionally.

3. CONCLUSIONS

Research conducted in this project provides new understanding into the role of membrane proteins in viral particle affinity and entry into cellular membranes. With the G attachment protein of the Nipah virus we found that cysteines in the stalk domain of NiV-G are not only important for maintaining the oligomeric stability of G, but also for proper folding of a unique subdomain located in the membrane distal region of the stalk that is necessary for F-triggering. These studies supplement our knowledge on the function of the stalk domain of paramyxovirus attachment proteins in F triggering, and identifies a critical microdomain that can be targeted for therapeutic or vaccine development. Precisely how membrane fusion between the viral particle and cell membrane occurs is poorly understood. Through model studies we found that steric pressure of membrane bound proteins confined to a lipid domain can drive curvature, a defining property of membrane undergoing fusion or fission. This work not only provides an understanding of protein-induced curvature in lipid membranes but also calls into question some of the long held theories of how membrane curvature is induced in endocytosis. We also show that protein-membrane interactions not only drive membrane curvature, but can also be defined by the curvature of the membrane itself. We have found that by using a nanoscale bump surface it is possible to selectively partition receptor molecules for protein affinity to specific sites in a membrane. Our efforts in understanding the relationship between protein assembly and membrane structure will further aid in the development of pathways to mitigate pathogen invasion and disease.

This page left blank intentionally.

4. REFERENCES

1) Maar, D.; Harmon, B.; Chu, D.; Schulz, B.; Aguilar, H. C.; Lee, B.; Negrete, O. A. *J. Virology* **2012**, *86*, 6632
2) Stachowiak, J. C.; Schmid, E. M.; Ryan, C. J.; Ann, H. S.; Sasaki, D. Y.; Sherman, M. B.; Geissler, P. L.; Fletcher, D. A.; Hayden, C. C. *Nature Cell Biology* **2012**, *14*, 944
3) Ogunyankin, M. O.; Huber, D. L.; Sasaki, D. Y.; Longo, M. L. *Langmuir* **2013**, *29*, 6109.
4) Lo, M. K., and P. A. Rota. 2008. The emergence of Nipah virus, a highly pathogenic paramyxovirus. *J Clin. Virol.* **2008**, *43*, 396-400.
5) Chua, K. B., K. J. Goh, K. T. Wong, A. Kamarulzaman, P. S. Tan, T. G. Ksiazek, S. R. Zaki, G. Paul, S. K. Lam, and C. T. Tan. *Lancet* **1999**, *354*,1257-1259.
6) Gurley, E. S., J. M. Montgomery, M. J. Hossain, M. R. Islam, M. A. Molla, S. M. Shamsuzzaman, K. Akram, K. Zaman, N. Asgari, J. A. Comer, A. K. Azad, P. E. Rollin, T. G. Ksiazek, and R. F. Breiman. *Infect. Control Hosp. Epidemiol.* **2007**, *28*, 740-742.
7) Lam, S. K., and K. B. Chua. *Clin. Infect. Dis.* **2002**, *34 Suppl 2***,** S48-51.
8) Field, H. E., J. S. Mackenzie, and P. Daszak. *Curr. Top Microbiol. Immunol*. **2007**, ***315,***133-159.
9) Luby, S. P., M. Rahman, M. J. Hossain, L. S. Blum, M. M. Husain, E. Gurley, R. Khan, B. N. Ahmed, S. Rahman, N. Nahar, E. Kenah, J. A. Comer, and T. G. Ksiazek. *Emerg. Infect. Dis.* **2006**, *12*,1888-1894.
10) Montgomery, J. M., M. J. Hossain, E. Gurley, G. D. Carroll, A. Croisier, E. Bertherat, N. Asgari, P. Formenty, N. Keeler, J. Comer, M. R. Bell, K. Akram, A. R. Molla, K. Zaman, M. R. Islam, K. Wagoner, J. N. Mills, P. E. Rollin, T. G. Ksiazek, and R. F. Breiman. *Emerg. Infect. Dis.* **2008**, *14*, 1526-1532.
11) Luby, S. P., E. S. Gurley, and M. J. Hossain. *Clin. Infect. Dis.* **2009**, *49*, 1743-1748.
12) Lamb, R. A., and T. S. Jardetzky. *Curr. Opin. Struct. Biol.* **2007**, *17*, 427-436.
13) Lamb, R. A., R. G. Paterson, and T. S. Jardetzky. *Virology* **2006**, *344*, 30-37.
14) Smith, E. C., A. Popa, A. Chang, C. Masante, and R. E. Dutch. *FEBS J.* **2009**, *276*, 7217-7227.
15) Bonaparte, M. I., A. S. Dimitrov, K. N. Bossart, G. Crameri, B. A. Mungall, K. A. Bishop, V. Choudhry, D. S. Dimitrov, L. F. Wang, B. T. Eaton, and C. C. Broder. *Proc Natl Acad Sci USA* **2005**, *102*, 10652-10657.

16) Negrete, O. A., E. L. Levroney, H. C. Aguilar, A. Bertolotti-Ciarlet, R. Nazarian, S. Tajyar, and B. Lee. *Nature* **2005**, *436,* 401-405.

17) Negrete, O. A., M. C. Wolf, H. C. Aguilar, S. Enterlein, W. Wang, E. Muhlberger, S. V. Su, A. Bertolotti-Ciarlet, R. Flick, and B. Lee. *PLoS Pathog* **2006**, *2,* e7.

18) Bowden, T. A., A. R. Aricescu, R. J. Gilbert, J. M. Grimes, E. Y. Jones, and D. I. Stuart. *Nat Struct Mol Biol* **2008**, *15,* 567-572.

19) Xu, K., K. R. Rajashankar, Y. P. Chan, J. P. Himanen, C. C. Broder, and D. B. Nikolov. Proc Natl Acad Sci USA **2008**, *105,* 9953-9958.

20) Bose, S., B. D. Welch, C. A. Kors, P. Yuan, T. S. Jardetzky, and R. A. Lamb. *J Virol.* **2001**, *85,* 12855 – 12866.

21) Yuan, P., K. A. Swanson, G. P. Leser, R. G. Paterson, R. A. Lamb, and T. S. Jardetzky. *Proc Natl Acad Sci USA* **2011**, *108,* 14920-14925.

22) Bishop, K. A., A. C. Hickey, D. Khetawat, J. R. Patch, K. N. Bossart, Z. Zhu, L. F. Wang, D. S. Dimitrov, and C. C. Broder. *J. Virol.* **2008**, *82,* 11398-11409.

23) Lee, J. K., A. Prussia, T. Paal, L. K. White, J. P. Snyder, and R. K. Plemper. *J Biol Chem* **2008**, *283,* 16561-16572.

24) McGinnes, L. W., and T. G. Morrison. *Virology* **1994**, *200,* 470-483.

25) Plemper, R. K., M. A. Brindley, and R. M. Iorio.. *PLoS Pathog* **2011**, *7,* e1002058.

26) Paal, T., M. A. Brindley, C. St Clair, A. Prussia, D. Gaus, S. A. Krumm, J. P. Snyder, and R. K. Plemper. *J Virol* **2009**, *83,* 10480-10493.

27) Feige, M. J.; Hendershot, L. M. *Curr. Opin. Cell Biol.* **2011**, *23,* 167 – 175.

28) Plemper, R. K., A. L. Hammond, and R. Cattaneo.. J Virol **2000**, *74,* 6485-6493.

29) Peter, B. J. *et al. Science* **2004**, *303,* 495-499.

30) Sweitzer, S. M.; Hinshaw, J. E. *Cell* **1998**, *93,* 1021 – 1029.

31) Lu, L., Ladinsky, M. S. & Kirchhausen, T. *Molec. Biol. Cell* **2009**, *20,* 3471-3480.

32) Wu, M. *et al. Nature Cell Biology* **2010**, *12,* 902-908.

33) Ford, M. G. *et al. Nature* **2002**, *419,* 361-366.

34) Lee, M. C. *et al. Cell* **2005**, *122,* 605-617.

35) Schmid, E. M. & McMahon, H. T. *Nature* **2007**, *448,* 883-888.

36) Xie, X., Cho, B. & Fischer, J. A. *Dev Biol* **2012**, *363,* 399-412.

37) Capraro, B. R., Yoon, Y., Cho, W. & Baumgart, T. *J. Am. Chem. Soc.* **2010**, *132,* 1200-1201.

38) Praefcke, G. J. *et al. EMBO J* **2004**, *23*, 4371-4383.

39) Rossman, J. S., Jing, X., Leser, G. P. & Lamb, R. A. *Cell* **2010**, *142*, 902-913.

40) Dibble, C. F. *et al. PLoS One* **2010**, *5*, e11740.

41) Fan, W., Nassiri, A. & Zhong, Q. *Proc Natl Acad Sci USA* **2011**, *108*, 7769-7774.

42) Saarikangas, J. *et al.*. *Curr Biol* **2009**, *19*, 95-107.

43) Ford, M. G. *et al. Science* **2001**, *291*, 1051-1055.

44) Drin, G. & Antonny, B. *FEBS Lett* **2010**, *584*, 1840-1847.

45) Campelo, F., McMahon, H. T. & Kozlov, M. M. *Biophys J* **2008**, *95*, 2325-2339.

46) Blood, P. D., Swenson, R. D. & Voth, G. A. *Biophys J* **2008**, *95*, 1866-1876.

47) Liu, A. P. & Fletcher, D. A. *Biophys J* **2006**, *91*, 4064-4070.

48) Tsafrir, I. *et al. Phys Rev Lett* **2001**, *86*, 1138-1141.

49) Yoon, Y. *et al. J Biol Chem* **2010**, *285*, 531-540.

50) Feder, J. *J Theor Biol* **1980**, *87*, 237-254.

51) Gizeli, E. & Glad, J. *Anal Chem* **2004**, *76*, 3995-4001.

52) Engelman, D. M. *Nature* **2005**, *438*, 578-580.

53) Veatch, S. L.; Keller, S. L. *Biochim. Biophys. Acta-Molec. Cell Res.* **2005,** *1746*, 172-185.

54) Marsh, D. *Biochim. Biophys. Acta-Biomembranes* **2009,** *1788*, 2114-2123.

55) Siegel, A. P.; Kimble-Hill, A.; Garg, S.; Jordan, R.; Naumann, C. A. *Biophys. J.* **2011,** *101*, 1642-1650.

56) Loew, M.; Springer, R.; Scolari, S.; Altenbrunn, F.; Seitz, O.; Liebscher, J.; Huster, D.; Herrmann, A.; Arbuzova, A. *J. Am. Chem. Soc.* **2010,** *132*, 16066-16072.

57) Nikolaus, J.; Scolari, S.; Bayraktarov, E.; Jungnick, N.; Engel, S.; Plazzo, A. P.; Stockl, M.; Volkmer, R.; Veit, M.; Herrmann, A. *Biophys. J.* **2010,** *99*, 489-498.

58) Yee, C. K.; Amweg, M. L.; Parikh, A. N. *Adv. Mater.* **2004,** *16*, 1184−1189

59) Shi, J. J.; Chen, J. X.; Cremer, P. S. *J. Am. Chem. Soc.* **2008,** *130*, 2718-2719

60) Yoon, T. Y.; Jeong, C.; Lee, S. W.; Kim, J. H.; Choi, M. C.; Kim, S. J.; Kim, M. W.; Lee, S. D. *Nat. Mater.* **2006,** *5*, 281-285.

61) Hoopes, M. I.; Faller, R.; Longo, M. L. *Langmuir* **2011,** *27*, 2783-2788.

62) Subramaniam, A. B.; Lecuyer, S.; Ramamurthi, K. S.; Losick, R.; Stone, H. A.. *Adv. Mater.* **2010,** *22*, 2142−2147

63) Sanii, B.; Smith, A. M.; Butti, R.; Brozell, A. M.; Parikh, A. N. *Nano Lett.* **2008,** *8*, 866-871.

64) Hsieh, W. T.; Hsu, C. J.; Capraro, B. R.; Wu, T. T.; Chen, C. M.; Yang, S.; Baumgart, T. *Langmuir* **2012,** *28,* 12838-12843

65) Ogunyankin, M. O.; Torres, A.; Yaghmaie, F.; Longo, M. L. *Langmuir* **2012,** *28,* 7107-7113.

66) Marsh, D. *Chem. Phys. Lipids* **2006,** *144,* 146-159

67) Meleard, P.; Gerbeaud, C.; Pott, T.; FernandezPuente, L.; Bivas, I.; Mitov, M. D.; Dufourcq, J.; Bothorel, P. *Biophys. J.* **1997,** *72,* 2616-2629.

68) Seitz, M.; Wong, J. Y.; Park, C. K.; Alcantar, N. A. *Thin Solid Films* **1998,** *327,* 767-771.

69) Svedhem, S.; Pfeiffer, I.; Larsson, C.; Wingren, C.; Borrebaeck, C.; Hook, F. *ChemBioChem* **2003,** *4,* 339-343

70) Darst, S. A.; Ahlers, M.; Meller, P. H.; Kubalek, E. W.; Blankenburg, R.; Ribi, H. O.; Ringsdorf, H.; Kornberg, R. D. *Biophys. J.* **1991,** *59,* 387-396.

71) Groves, J. T.; Wulfing, C.; Boxer, S. G. *Biophys. J.* **1996,** *71,* 2716-2723.

72) Shnek, D. R.; Pack, D. W.; Sasaki, D. Y.; Arnold, F. H. *Langmuir* **1994,** *10,* 2382-2388.

73) Schmitt, L.; Bohanon, T. M.; Denzinger, S.; Ringsdorf, H.; Tampe, R. *Angew. Chem.-Int. Ed. Engl.* **1996,** *35,* 317-320.

74) Hayden, C. C.; Hwang, J. S.; Abate, E. A.; Kent, M. S.; Sasaki, D. Y. *J. Am. Chem. Soc.* **2009,** *131,* 8728-8729.

75) Stachowiak, J. C.; Hayden, C. C.; Sanchez, M. A. A.; Wang, J.; Bunker, B. C.; Voigt, J. A.; Sasaki, D. Y. *Langmuir* **2010,** *27,* 1457-1462.

76) Stachowiak, J. C.; Hayden, C. C.; Sasaki, D. Y. *Proc. Natl. Acad. Sci. USA* **2010,** *107,* 7781-7786.

77) Stachowiak, J. C.; Schmid, E. M.; Ryan, C. J.; Ann, H. S.; Sasaki, D. Y.; Sherman, M. B.; Geissler, P. L.; Fletcher, D. A.; Hayden, C. C. *Nat. Cell Biol.* **2012,** *14,* 944-949

78) Jensen, M. H.; Morris, E. J.; Simonsen, A. C. *Langmuir* **2007,** *23,* 8135-8141

DISTRIBUTION

1 Prof. Jeanne C. Stachowiak
Dept. of Biomedical Engineering
BME 5.202G, MC C0800
The University of Texas at Austin
Austin, TX 78712

1	MS9055	Carl Hayden	8353
1	MS9292	Oscar Negrete	8621
1	MS9671	Ryan Davis	8634
1	MS9292	Darryl Sasaki	8621
1	MS0899	Technical Library	9536 (electronic copy)
1	MS0359	D. Chavez, LDRD Office	1911


Sandia National Laboratories